4-1-2009

The Role of the Trivalent metal in an LDH: Synthesis, Characterization and Fire Properties of Thermally Stable PMMA/LDH Systems

Charles Manzi-Nshuti
Marquette University

Dongyan Wang
Marquette University

Jeanne Hossenlopp
Marquette University, jeanne.hossenlopp@marquette.edu

Charles A. Wilkie
Marquette University, charles.wilkie@marquette.edu

Accepted version. *Polymer Degradation and Stability*, Vol. 94, No. 4 (April 2009): 705-711. DOI.

The Role of the Trivalent metal in an LDH: Synthesis, Characterization and Fire Properties of Thermally Stable PMMA/LDH Systems

Charles Manzi-Nshuti
Department of Chemistry and Fire Retardant Research Facility, Marquette University
Milwaukee, WI
Dongyan Wang
Department of Chemistry and Fire Retardant Research Facility, Marquette University
Milwaukee, WI
Jeanne M. Hossenlopp
Department of Chemistry and Fire Retardant Research Facility, Marquette University
Milwaukee, WI
Charles A. Wilkie
Department of Chemistry and Fire Retardant Research Facility, Marquette University
Milwaukee, WI

Abstract: *Two layered double hydroxides (LDHs), calcium aluminum undecenoate (Ca_3Al) and calcium iron undecenoate (Ca_3Fe), have been prepared by the co-precipitation method. XRD analysis of these LDHs*

Polymer Degradation and Stability, Vol. 94, No. 4 (April 2009): pg. 705-711. DOI.

reveals that they are layered materials and FT-IR and TGA confirmed the presence of the undecenoate anions in the material produced. The PMMA composites were prepared by bulk polymerization and the samples were characterized by XRD, TEM, TGA and cone calorimetry. Both additives greatly enhance the thermal stability of PMMA, while the calcium aluminum LDH gives better results when the fire properties were examined using the cone calorimeter.

1. Introduction

Many investigations have shown that inorganic hydroxide fillers, especially magnesium hydroxide (MH) and aluminum trihydrate (ATH) are environmentally friendly additives [1,2]. However, they have disadvantages, such as the need for quite high loadings and poor compatibility with the polymeric matrix, which degrade the mechanical properties [3]. The search for other inorganic hydroxide to substitute for existing metal hydroxides (MH, ATH) has been of current interest [4].

In previous observations on polymer-clay nanocomposite flammability using montmorillonite (MMT) as the nanodimensional material, it is observed that reduction in the peak heat release rate (PHRR) is dependent on the polymer matrix and the quality of the nano-dispersion. In the case of polystyrene (PS), polyamide-6 (PA-6) and ethylene vinyl acetate copolymer (EVA), the reduction in PHRR is quite significant, around 60% [5]. However, in the case of poly(methyl methacrylate) (PMMA), only a modest reduction in PHRR, 30%, can be achieved [6,7]. It was further observed that the typical small reduction in PHRR seems to be dependent on both the identity and amount of the surfactant [8,9].

The small reductions in PHRR observed for MMT/PMMA systems triggered a search for new additives for this polymer. Layered double hydroxides (LDHs), also known as hydrotalcite-like materials, may be a good candidate for this, as the composition of the layers can be varied, which is not possible with an MMT-like material. This presents an advantage, since tuning the LDH may lead to enhancement in some properties, but a good understanding of the role of each component of the LDH is required for optimization of the properties.

Polymer Degradation and Stability, Vol. 94, No. 4 (April 2009): pg. 705-711. DOI.

The LDH structure is described with the ideal formula $[M^{II}_{1-x}M^{III}_{x}(OH)_2]_{intra}[A_{x/m}{}^{m-}\cdot nH_2O]_{inter}$, where M^{II} is a divalent cation such as Mg, Co, Ni, Cu, or Zn and M^{III} is a trivalent cation such as Al, Cr, Fe, V, or Ga with $A_{x/m}{}^{m-}$ an anion of charge m such as NO_3^-, CO_3^{2-}, Cl^-, SO_4^{2-}, $C_{12}H_{25}SO_4^-$, various carboxylates, etc; intra and inter denote the intralayer domain and the interlayer space, respectively. The LDH structure consists of brucite-like layers constituted of edge-sharing $M(OH)_6$ octahedra [10].

Anionic guest entities, like monomers and polymers [11,12], functional biomolecules [13,14], and complexes of reducible transition metals [15,16] have been intercalated within an LDH matrix. LDH nanocomposites have found applications in mechanical strengthening [11,12], as adsorbents [17], or magnetic nanostructures [15,16]. In contrast, their potential usage as fire retardants has not been widely explored.

In recent work on LDHs as fire retardants for polymers, it was observed that matching an LDH with a particular polymer is a key to use these nanomaterials effectively [18]. An Mg-Al LDH will disperse much better in a polar polymer, like PMMA, than in a non-polar polyethylene, polypropylene or polystyrene. This task is not simple, as there are many parameters to control: metals (divalent and trivalent), anion functional groups (carboxylate, solfonate, sulfate, phosphate, etc.), anion sizes, crystallite sizes, stoichiometry and the polymer. The variation of the divalent metal cation in an LDH has an influence dispersability and fire properties of the corresponding polymer (nano)composites [19]. Finally, the length of the carboxylate chain has been varied and the dispersability of the LDH and fire properties assessed with both PMMA and PS; the dispersion is much better with PMMA but there is still a substantial reduction in the peak heat release rate even with the LDH poorly dispersed in PS [20]. In this work, two trivalent metal ions, aluminum and iron, are used keeping the divalent metal and anion the same.

There are a few reports in the literature discussing the use of iron in the fire retardancy of polymers. Nangrani et al. [21] reported that ferric oxide actually increased the flammability of polycarbonate.

Polymer Degradation and Stability, Vol. 94, No. 4 (April 2009): pg. 705-711. DOI.

Whelan [22) investigated iron oxide as an effective synergist with halogens in halogen-containing nitrile polymers. Recently, Jiao et al. [4] reported that EVA/(Mg/Al/Fe-CO_3) composites containing a variable amount of Fe^{3+} ion obtained a V-0 rating in the UL-94 protocol, while with EVA/MgAl-CO_3,(an iron-free hydrotalcite), dripping occurred. The presence of iron as a substitutional impurity in MMT has been shown to lead to radical trapping reactions and a reduction in the PHRR at low amounts of clay [23]. Kong et al. have recently reported on a synthetic iron-containing MMT analog and found that the iron has a significant effect on the degradation and fire properties [24].

2. Experimental

2.1. Materials

The materials used in the synthesis of the layered double hydroxides were analytical grade, obtained from the Aldrich Chemical Co. These include 10-undecenoic acid, $Ca(NO_3)_2{\cdot}4H_20$, $Al(NO_3)_3{\cdot}9H_20$, $Fe(NO_3)_3{\cdot}6H_2O$, sodium hydroxide. Methyl methacrylate (MMA) and benzoyl peroxide (BPO) were used to prepare the polymer composites. MMA monomer was passed through an inhibitor remover column before use.

2.2. Preparation of the LDHs

The Ca/Al and Ca/Fe LDHs undecenoate were synthesized using the co-precipitation method following the literature procedure [25]. The preparation was performed in a nitrogen atmosphere to exclude CO2 from the LDHs: 2000 ml of deionized water was boiled for 30 min while purging with nitrogen, then cooled to room temperature. In a 3 L three-neck flask was placed 900 ml of the previously treated water, under a constant nitrogen flow. To this was added 50 g (0.27 mol) of undecenoic acid and 5 min later, 11 g (0.27 mol) of NaOH. After the solution became colorless, the nitrate solution was prepared in separate container by dissolving 64 g (0.27 mol) of calcium nitrate and 34 g (0.091 mol) of aluminum nitrate in 450 ml of previously boiled water. This solution was then added dropwise to the 10-undecenoate solution, maintaining the pH of the solution at 10.0 ± 0.1. The slurry was aged at 60 °C for 2 days, and washed several times with

degassed deionized water and dried in a vacuum oven at 80 °C for a day to yield the desired calcium aluminum undecenoate LDH (Ca_3Al). Ca_3Fe was obtained similarly, with iron nitrate replacing aluminum nitrate and this sample was aged at room temperature.

2.3. Preparation of LDHs/PMMA nanocomposites

The PMMA/LDHs nanocomposites were prepared by a two-stage process by in situ bulk polymerization as reported by Wang et al. [25] with minor modifications. Briefly, the appropriate LDH loading was combined with MMA, total weight 140 g in a 400 ml beaker covered with aluminum foil to reduce volatilization, and the mixture was stirred vigorously for 1 day. Then, the initiator, BPO, 0.1% was added, and the mixture heated to 70 °C to pre-polymerize it. The viscous mixture was cooled until a critical viscosity was reached, and another portion of initiator, 0.1% (0.14 g) was added to the viscous mixture, which was then heated to 120°C for 8 h. At the end, the polymer was placed overnight in a vacuum oven at 100 °C to remove unreacted monomer and yield the LDH/PMMA nanocomposites. For the two types of LDHs prepared in this study, the LDH loadings used with PMMA were 1, 5, and 10%. This two-stage process was also used for the preparation of the control PMMA sample.

2.4. Determination of molecular weight by viscosity

The molecular weight of PMMA used in this work was obtained from viscosity data. The results are an average of three determinations, and the Mark-Houwink constants were obtained from published data [26].

2.5. Characterization

Thermogravimetric analysis (TGA) was performed on an SDT 2960 (TA Instruments) at the 15 mg scale under a flowing nitrogen atmosphere at a scan rate of 20 °C/min. Temperatures are reproducible to ±3 °C, while the error on the fraction of non-volatile materials is ±2%. TGA was done in duplicate and the average values are reported. Fourier transform infrared (FT-IR) spectra of the solid materials were obtained using the ATR mode on a Nicolet Magna-IR

560 spectrometer operated at 1 cm^{-1} resolution in the 650-4000 cm^{-1} region. X-ray diffraction (XRD) measurements of the LDHs were performed on a Bruker-Nonius APEX2 with CCD detector with 0.5 mm Monocap collimator and graphite monochromator with Cu Kα generator (λ = 1.54078 Å) from a sealed X-ray tube. The powder sample was prepared as a 0.3 mm ball using a small amount of mineral oil and was put on the top of 0.1 mm nylon pin. The data were collected at various 2*θ* values in 9° increments using 180° Φ rotations. The polymeric samples were compression molded into 20 mm × 15 mm × 1 mm plaques for XRD measurements on a Rigaku Miniflex II X-ray diffractometer, scaning from 1° to 10° at 0.02° step size.

Bright field transmission electron microscopy (TEM) images of the composites were obtained at 80 kV with a Zeiss 10c electron microscope. The samples were ultramicrotomed with a diamond knife on a Riechert-Jung Ultra-Cut E microtome at room temperature to give ~70 nm thick sections. These sections were transferred from a knife-edge to 600 hexagonal mesh Cu grids. Cone calorimeter measurements were performed on an Atlas CONE-2 according to ASTM E 1352 at an incident flux of 50 kW/m^2, using a cone shaped heater; the exhaust flow was set at 24 L/s. The specimens for cone calorimetry were prepared by compression molding of the sample (about 30 g) into 3 × 100 × 100 mm square plaques. Typical results from cone calorimetry are reproducible to within about ± 10%; these uncertainties are based on many runs in which thousands of samples have been combusted [27].

3. Results and Discussion

XRD patterns of the two LDHs, Ca_3Al and Ca_3Fe are shown in Fig. 1. The layer structure of the Ca_3Al is more pronounced as the diffraction peaks are more symmetrical and sharp. The Ca_3Fe produced under similar condition is also a layered material, as noted from the presence of two other reflection peaks at equidistant 2*θ* values, but it was poorly crystallized, as noted from the asymmetric shape of the diffraction peaks. The basal spacing is about 3 nm for both LDHs, indicating that the undecenoate anions were successfully intercalated between the layers.

Fig. 2 provides the TGA of Ca_3Al and Ca_3Fe, in a nitrogen environment, run from 50 to 600 °C. Both materials show a mass loss below 150 °C, assigned to the loss of gallery water. DTA of both materials (Fig. 3) shows that this mass loss is endothermic, centered around 130 °C. When heated to higher temperature, several other events are visible in the TGA/DTG curves. The other events are probably due to the dehydroxylation of the layers and total decomposition of the materials; this is the normal observation for an LDH [28]. The loss of the organic moiety occurs earlier for Ca 3Fe compared to Ca3Al. This is shown by the sharp DTG peak around 425 °C and an exothermic DTA event (max 450 °C) for Ca3Fe while a similar event is observed at 475 °C (DTG) and 492 °C (DTA) for Ca3Al. The degradation of Ca3Fe is complete earlier (475 °C) than that of Ca3Al (513 °C). The final mass remaining is 47% and 34% for Ca3Fe and Ca3Al, respectively. From calculations based on the amount of reagents used and expected LDH formulae, a final mass of 47% and 44% is expected for Ca3Fe and Ca3Al, respectively, which indicates that Ca3

Further characterization of the LDHs used FT-IR (Fig. 4). With both materials, the observed bands are characteristic of undecenoate-containing LDHs, and the assignments of the various bands correlate very well to previous work on undecenoate-containing LDH with different divalent metals [19]. The carbonate anion, the usual contaminant of these materials, is not present as shown by the absence of a peak at 1360 cmAl produced contains excess organic. -1. An additional band, a sharp band around 1578 cm-1 is also observed in these spectra and can be attributed to the asymmetric uc=o of a hydrogen-bonded carboxylic acid in the interlayer of the LDH material [28,29]. The intercalation of such free acid groups [30] is a general phenomenon when excess carboxylate anions are used in the exchange or preparation, even at such high pH [31]. Overall, XRD, TGA/DTA and FT-IR of these two LDHs confirm that layered materials, containing undecenoate anions intercalated in the gallery spacing of the LDHs, have been produced.

Nanocomposites can be described as immiscible, intercalated or exfoliated depending on the type of dispersion of the polymer matrix in the layers of the nanomaterial. In an immiscible system, also called a micro composite, the polymer does not enter into the gallery space of the nanomaterial; this is a conventional composite. An intercalated nanocomposite is obtained when the polymer enters the gallery space and the registry between the layers is maintained. In an exfoliated system, also referred to as a delaminated system, excellent nano-dispersion of the layered material into the polymer matrix is accompanied with a loss of the registry between the layers. Wide-angle X-ray diffraction (XRD) and transmission electron microscopy (TEM) are the most commonly used methods to study the dispersion of the polymer matrix into the galleries of the inorganic material.

After bulk polymerization of MMA/LDH, the diffraction peaks disappeared at all loadings (1, 5, 10%) and for both Ca3Al/(Fig. 5) and Ca3Fe/composites (Fig. 6). Two extreme cases can explain the disappearance of the diffraction peaks in XRD: (1) complete exfoliation of the layers in the polymer matrix, and/or (2) disordering of the LDH layers within the polymer matrix with no change in the d-spacing. To obtain more insight into the morphology of the PMMA/LDHs, TEMs were obtained and are shown in Figs. 7 and 8.

The TEM images of PMMA/5%Ca_3Fe are shown in Fig. 7. The lower magnification image on the left shows agglomeration of smaller tactoids dispersed unevenly in the polymer matrix. At higher magnification, the tactoids are still seen grouped into a circular disk without the presence of individual layers; hexagonal platelets, typical of pristine LDH, are also observed. Overall, this TEM suggests poor dispersion of this LDH within the PMMA matrix. The TEM image of PMMA/5%Ca_3Al on the other hand (Fig. 8) shows a different morphology. The low magnification image shows fair dispersion of the LDH within the polymer matrix. The higher magnification image reveals that the registry of some of the layers is maintained, but also individual exfoliated layers are visible. Overall, a mixed intercalated-exfoliated morphology is suggested.

The thermal degradation pathways of PMMA are well understood. When PMMA is heated, the first small mass loss observed

is due to cleavage of weak links, typically head-to-head linkages [32], followed by larger mass loss due to scission at the unsaturated ends formed through termination by disproportionation. The final main event is the random chain scission of the PMMA backbone [33].

The TGA and corresponding derivatized mass, DTG, curves of PMMA and its Ca_3Fe composites heated in nitrogen from 100 to 600°C are shown in Figs. 9 and 10, respectively, and the TGA data (onset temperature of degradation, $T_{0.1}$, midpoint degradation temperature, $T_{0.5}$and the char at 600 °C) are summarized in Table 1. The presence of the LDH pushes the TGA curves of the composites to higher temperatures showing enhanced thermal stability relative to the pure polymer.

The composites and the control polymer all show the two main thermal events expected for PMMA. The normal first step of degradation of PMMA, due to weak linkages, is not clearly observed in these samples. The event attributed to the scission at the unsaturated chain end is less pronounced when the LDH is added to the PMMA matrix. The molecular weight of the control PMMA sample obtained by viscosity measurement was 336,600 ± 8700. It should be pointed out that other factors, like the molecular weight of the polymer in a PMMA/LDH system can also play an important role in the properties of the system. Work is underway to elucidate this possibility. The main degradation event, the random scission of the PMMA backbone, occurs at a higher temperature relative to the virgin polymer prepared under similar conditions. T_{max} is around 400n °C for all PMMA/Ca_3Fe composites while that for pure PMMA is at 373 °C.

The TGA and corresponding derivatized mass, DTG, curves of PMMA and its Ca_3Al composites heated in nitrogen from 100 to 600 °C are shown in Figs. 11 and 12, respectively, and the TGA data (onset temperature of degradation, $T_{0.1}$ midpoint degradation temperature, $T_{0.5}$ and the char at 600 °C) are summarized in Table 1. As the LDH loading is increased, the thermal stability of the composite is gradually enhanced. Also, as summarized in Table 1, the char obtained at the end of the experiment gradually increases, and the mass of the char agrees well with that expected based on the amount of LDH.

The main difference between the thermal behavior of Ca_3Al and Ca_3Fe is noted in the last step associated with random chain scission of the PMMA backbone. As the Ca_3Al loading increases, both $T_{0.5}$ and T_{max} increase as the loading of the LDH increases while for the iron-containing material, T_{max} does not depend upon loading of the LDH and $T_{0.5}$ is 12 °C higher at 1% loading compared to the aluminum-containing system. Both additives, Ca_3Fe and Ca_3Al, offer significant enhancement in thermal stability of the PMMA composites relative to the pure polymer.

The fire properties of the PMMA/LDH systems were measured by cone calorimetry. Important parameters obtained from such a test are: time to ignition, amount of smoke produced, average mass loss rate, total heat released, the heat release rate and especially its peak value (PHRR). The reduction in PHRR is important for fire safety, as PHRR represents the point in a fire where heat is likely to propagate further, or ignite adjacent objects [34].

Fig. 13 provides the HRR curves of PMMA and its Ca_3Fe composites while Fig. 14 gives the HRR curves of PMMA/Ca_3Al systems. The summary of the cone calorimetric data is provided in Table 2. Overall, increasing the additive loading from 1 to 10% enhances the fire properties of the composites, shown by a gradual decrease in PHRR for all systems. The greatest reduction (54%) is obtained with PMMA/10% Ca_3Al sample. Bearing in mind that typical reductions observed for PMMA/MMT nanocomposites are usually in the range of 30% [7], these PMMA/LDH systems are very effective. Comparing the aluminum-containing samples with iron-containing samples, the former gives greater reductions in PHRR and burn for a longer time relative to the iron-containing systems and the virgin polymer. The TEM images of the two systems reveal relatively good dispersion for the PMMA/5%Ca_3Al system while poor dispersion was noted for PMMA/5%Ca_3Fe sample. While one may be tempted to conclude that the metals play a role in the type of reduction obtained in these samples, the differences in the degree of dispersion may also explain the differences in the fire properties. Attempting to better

disperse the iron-containing LDH in PMMA and comparing this new system with the PMMA/Ca_3Al system should be the next challenging experiment in order to elucidate the dependence on the trivalent metal.

In previous work with various polymer/LDH systems, we have seen that there is not a good correlation between the nano-dispersion and cone calorimetry results. In several cases, it was observed that even a poorly dispersed LDH/polymer system gives as large a reduction in the PHRR as seen for a well-dispersed system [18-20]. This is completely unlike what has been seen for MMT systems where only well-dispersed clay gives a reduction in the PHRR. This continues to be a topic of interest in these laboratories.

The effectiveness of PMMA/10%Ca_3Al composites can be compared with fire behavior observed with polymer-MMT nanocomposites [6] where the nanocomposites burn for a longer time, but since the fuel is released slowly, the HRR stays low throughout the burning process. The finding that iron-containing LDH/PMMA system giving a higher PHRR relative to aluminum-containing LDH/ PMMA can, however, be correlated to the data reported by Jiao et al. [4] where their Mg/Al/Fe-CO_3 LDHs (sample containing a higher concentration of Fe3+) had a higher PHRR value relative to similar materials with lower iron content. From the same work, it was observed that the introduction of Fe3+ into the LDH prevented dripping in the EVA/(Mg/Al/Fe-CO3 LDH) composites and improved the UL-94 ratings. Also, from Table 2, the iron-containing PMMA systems produce less smoke relative to the aluminum analogs at similar additive loading.

4. Conclusions

Two layered double hydroxides have been prepared and used to prepare thermally stable PMMA composites. We successfully prepared two layered materials intercalated with 10-undecenoate anions. The iron-containing LDH used in this investigation was less crystalline relative to its aluminum analog, but both materials give promising results when combined with PMMA. Greater reduction in PHRR (54%) was recorded with PMMA/10% Ca3Al sample with PMMA/10%Ca3Fe giving 34%. While the major difference between the two systems is

the metals, aluminum versus iron, it was noted that the dispersion was quite different, and the next challenge is to produce a well-dispersed iron-containing PMMA/LDH system and evaluate the corresponding fire and thermal properties to compare with this data.

Acknowledgments: This work was performed under the sponsorship of the US Department of Commerce, National Institute of Standards and Technology, Grant 60NANB6D6018.

References

[1] Lv JP, Qui IZ, Qu BJ. Nanotechnology 2004;15:1576.
[2] Fu MZ, Qu BJ. Polym Degrad Stab 2004;85:633.
[3] Wang ZZ, Qu BJ, Fan WC, Huang P. J Appl Polym Sci 2001;81 :206.
[4] Jiao CM, Wang ZZ, Chen X, Hu Y. J Appl Polym Sci 2008;107:2626.
[5] Marosföi BB, Marosi GJ, Szep A, Anna P, Keszei S, Nagy BJ, et al. Polym Adv Technol 2006;17:255.
[6] Morgan AB. Polym Adv Technol 2006;17:206.
[7] Costache MC, Wang D, Heidecker MJ, Manias E, Wilkie CA. Polym Adv Technol 2006;17:272.
[8] Zhu J, Start P, Mauritz KA, Wilkie CA. Polym Degrad Stab 2002;77:253.
[9] Jash P, Wilkie CA. Polym Degrad Stab 2005;88:401.
[10] Hofmeister W, Von Platen H. Cryst Rev 1992;3:3; Bender-Koch C. Hyperfine Interact 1998;117:131.
[11] Leroux F, Taviot-Gueho C. J Mater Chern 2005;15:3629.
[12] Darder M, Lopez-Blanco M, Aranda P, Leroux F, Ruiz-Hitzky E. Chern Mater 2005;17:1969.
[13] Ambrogi V, Fardella G, Grandolini G, Perioli L IntJ Pharm 2001;220:22.
[14] Nakayama H, Wada N, Tsuhako M. Int J Pharm 2004;269:469.
[15] Tsyganok A, Sayari A. J Solid State Chern 2006;179:1830.
[16] Tarasov KA, O'Hare D, Isupov VP. Inorg Chern 2003;42:1919.
[17] Dékàny I, Berger F, Imrik K, Lagaly G. Colloid Polym Sci 1997;275:681.
[18] Nyambo C, Wang D, Wilkie CA. PolymAdvTechnol, in press.doi: 1O.1001/pat.1272.
[19] Manzi-Nshuti C, Wang D, Hossenlopp JM, Wilkie CA. J Mater Chern 2008;18:3091-102.
[20] Nyambo C, Songtipya P, Manias E, Jimenez-Gasco MM, Wilkie CA. J Mater Chern. 2008; 18: 4827-38. doi: 10.1039/b806531d.
[21] Nangrani KJ, Wenger R, Daugherty PG. Plast Compd 1988;11 :2729.
[22] Whelan WP. J Fire Ret Chern 1979;6:206.
[23] Zhu J, Uhl F, Morgan AB, Wilkie CA. Chern Mater 2001;13:4649-54.

[24] Kong Q, Hu Y, Song L, Wang Y, Chen Z, Fan W. Polym Adv Technol 2006;19:463-7. Hu Y. Yang D. Song L. Polym Mater Sci Eng 2008;98:766.
[25] Wang G-A, Wang C-C, Chen C-c. Polymer 2005;46:5065.
[26] Kurata M, Tsunashima Y. In: Brandrup J, Immergut EH, Grulke EA, editors. Polymer handbook. 4th ed. New York: Wiley; 1999. p VII 1-83.
[27] Gilman JW, Kashiwagi T, Nyden M, Brown JET, Jackson CL, Lomakin S, et al. In: Al-Malaika S, Golovoy A, Wilkie CA. editors. Chemistry and technology of polymer additives. Oxford: Blackwell Scientific; 1999. p. 249.
[28] Xu ZP, Braterman PS, Yu K, Xu H, Wang Y, Brinker CJ. Chern Mater 2004;16:2750.
[29] Borja M, Dutta PK. J Phys Chern 1992;96:5434.
[30] Kloprogge JT, Frost RL. J Solid State Chern 1999;146:506.
[31] Xu ZP, Braterman PS, Seifollah N. Abstract. In: Proceedings of the 224th ACS National Meeting. Boston. MA. Aug. 18-22; 2002. Coli. 219.
[32] Holland BJ, Hay IN. Polym Degrad Stab 2002;77:435.
[33] Kashiwagi T, Inaba A, Brown JE, Hatada K, Kitayama T, Masuda E. Macromolecules 1986;19:2160.
[34] Babrauskas V, Peacock RD. Fire Safety J 1992;18:255.

Appendix

Figure 1: XRD patterns of Ca_3Al and Ca_3Fe LDHS-undecenoate

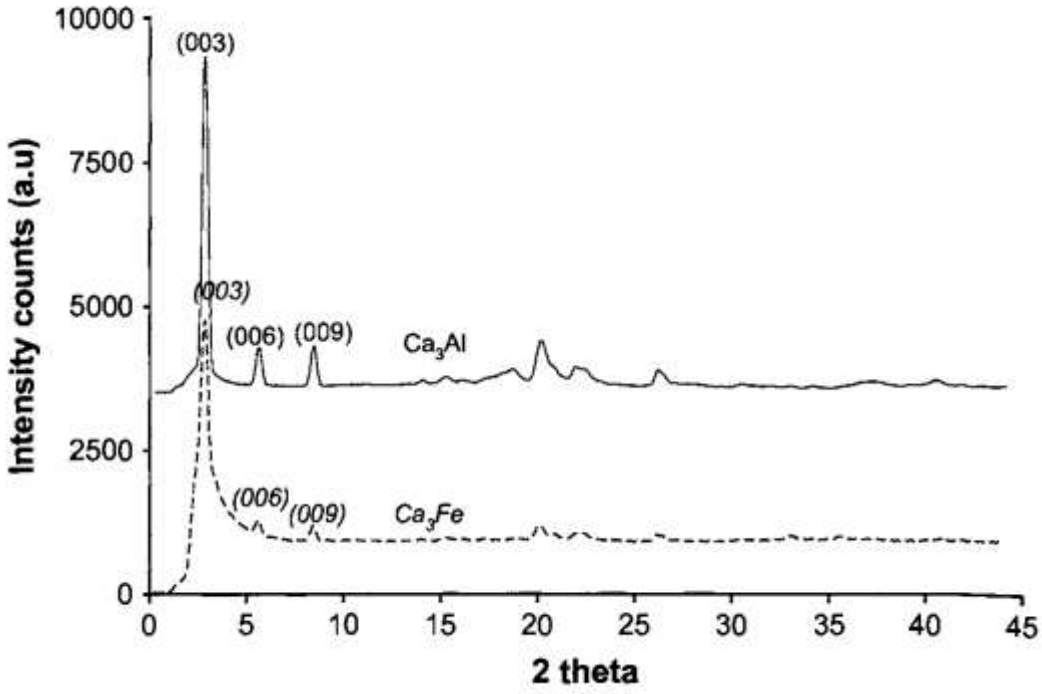

Figure 2: TGA and DTG profiles of undecenoate-LDHs. (A) Ca_3Fe LDH; (B) Ca_3Al LDH.

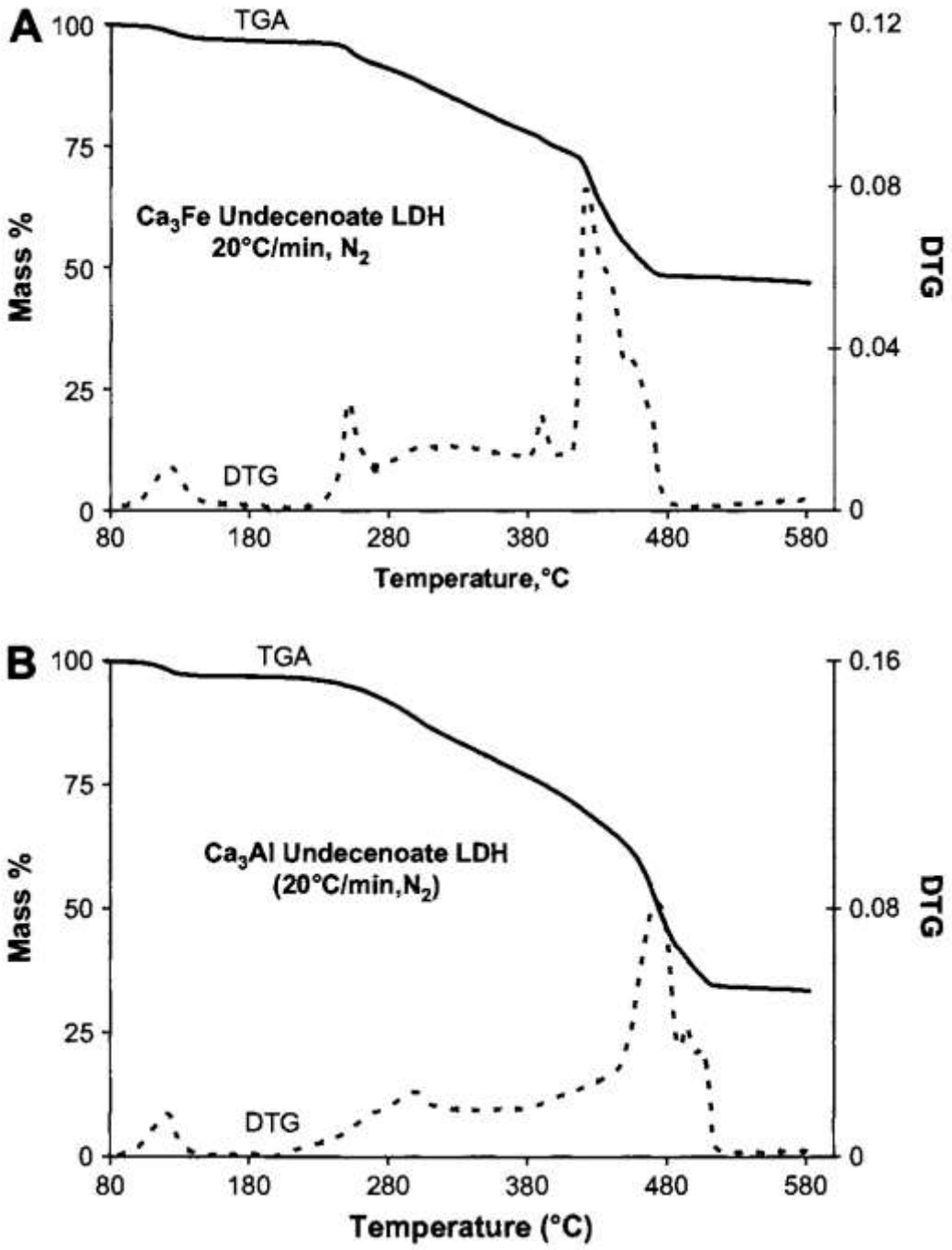

Figure 3: DTA profiles of Ca_3Al LDH (solid line) and Ca_3Fe LDH (dashed line).

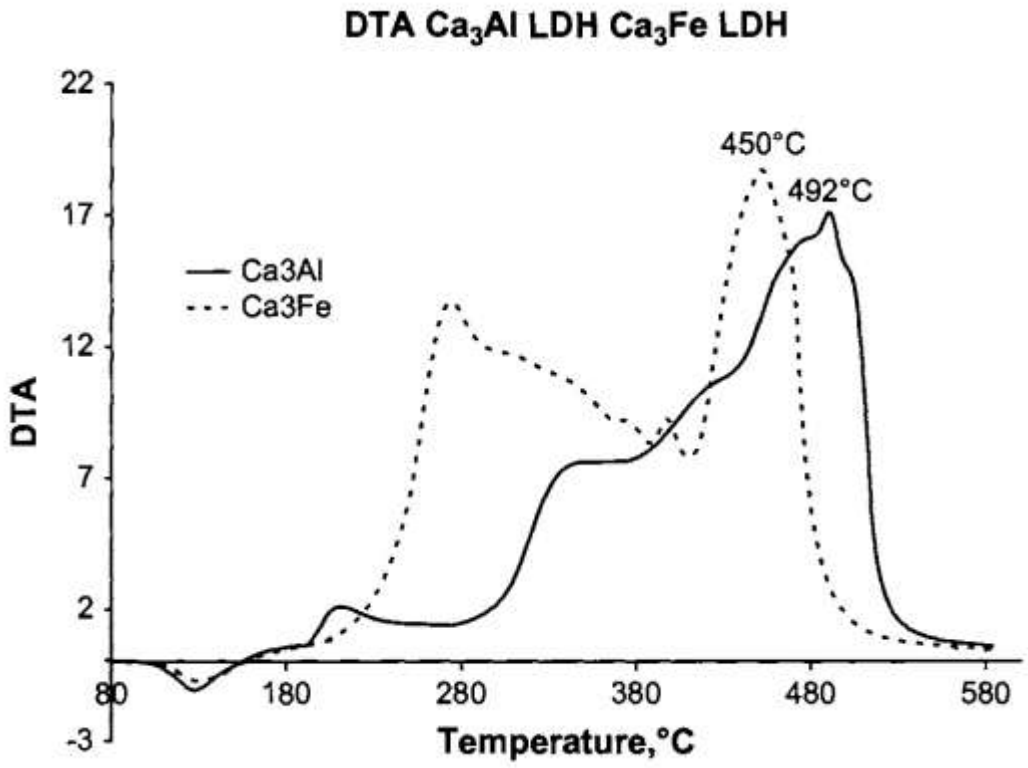

Figure 4: FT-IR of Ca_3Al LDH and Ca_3Fe LDH (ATR mode).

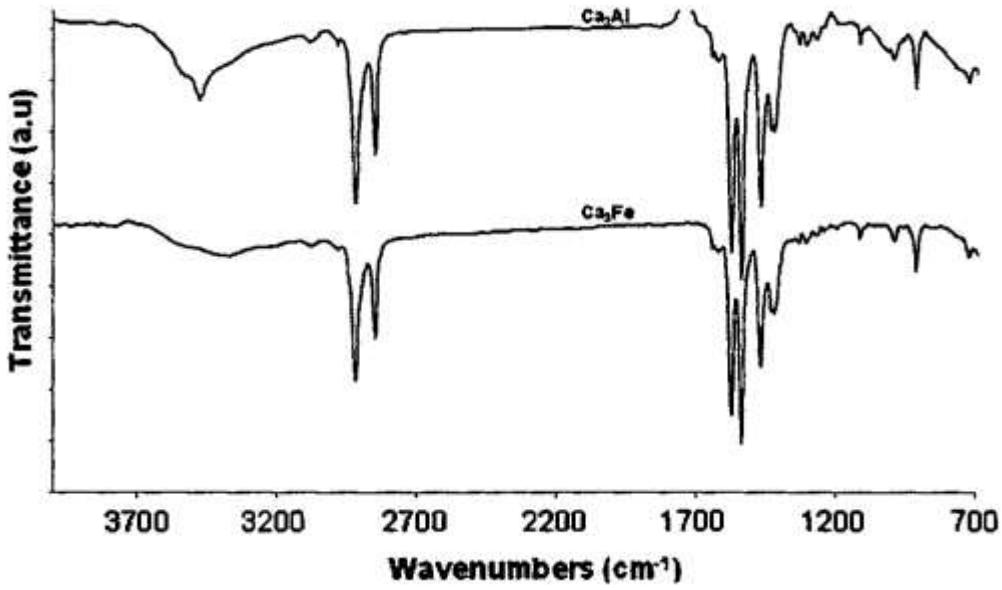

Figure 5: XRD traces of Ca_3Al LDH and its PMMA composites.

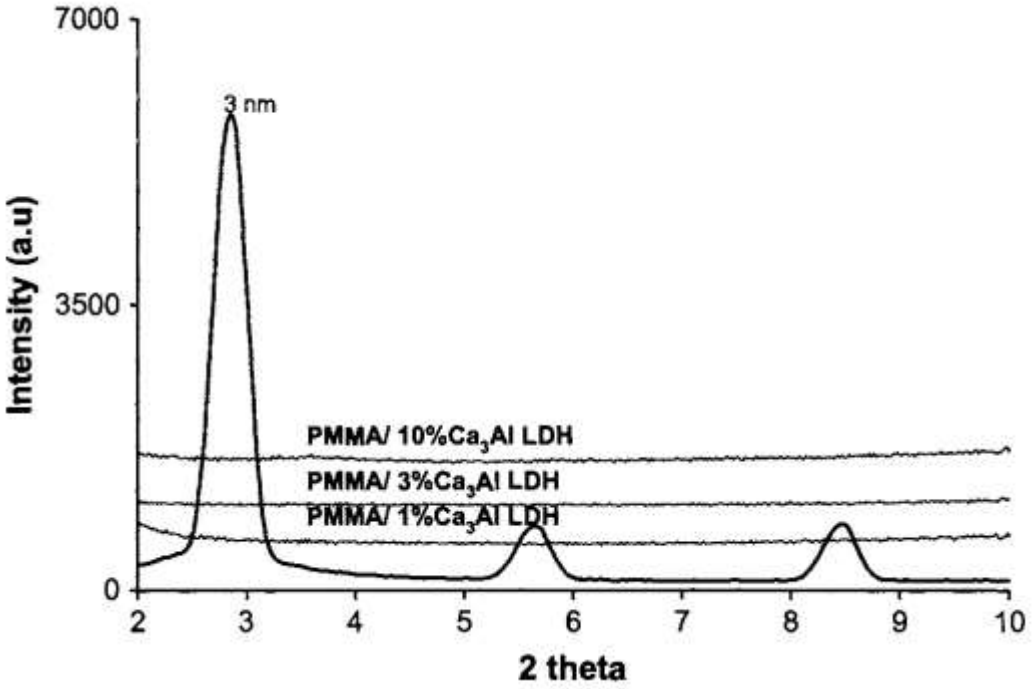

Figure 6: XRD traces of Ca_3Fe LDH and its PMMA composites.

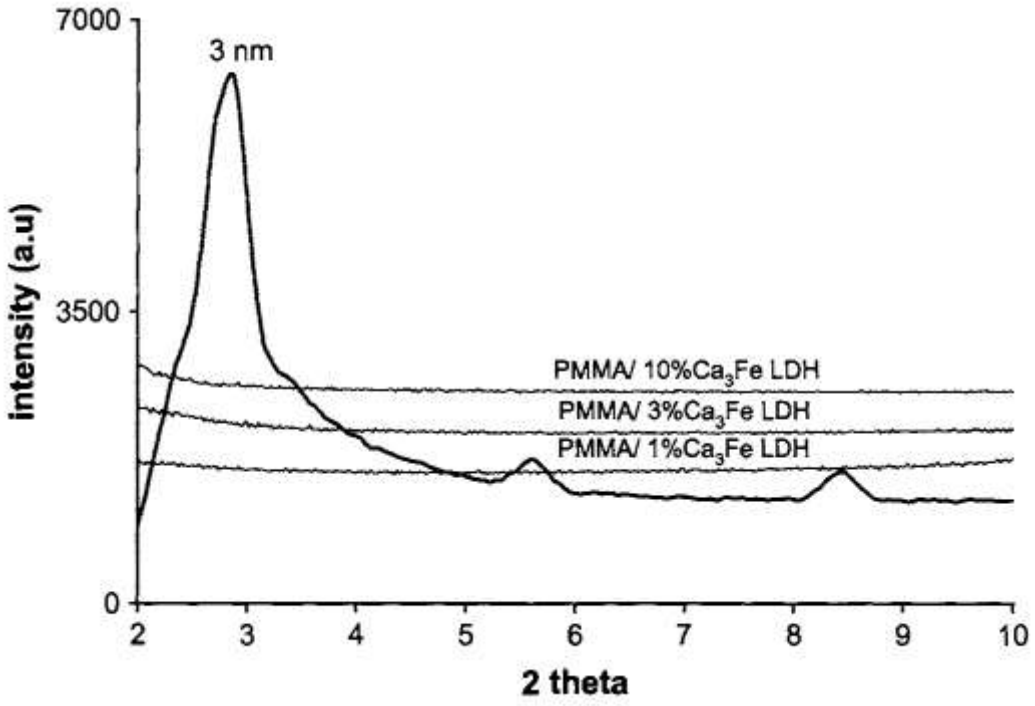

Figure 7: TEM image of PMMA/Ca_3Fe LDH at different magnifications.

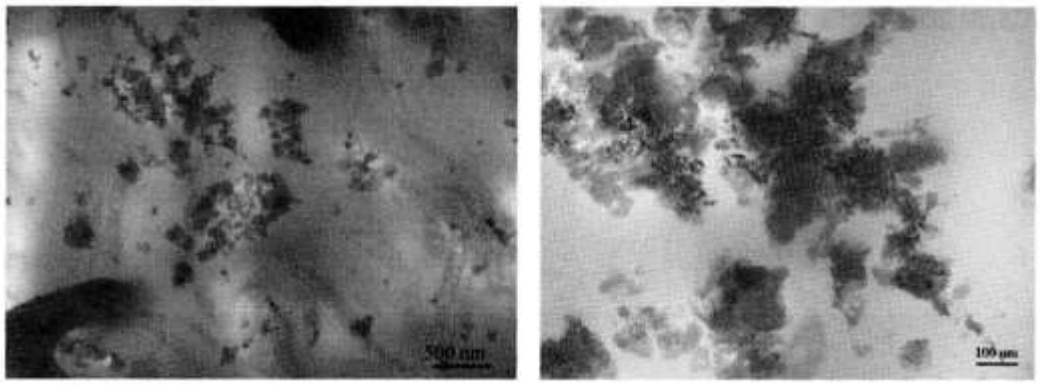

Figure 8: TEM image of PMMA/Ca_3Al LDH at different magnifications.

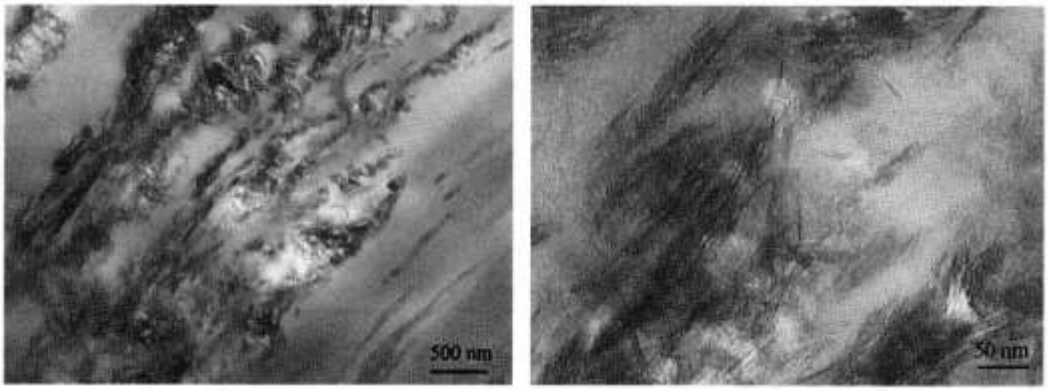

Figure 9: TGA curves of PMMA and its Ca_3Fe undecenoate composites. (A) PMMA; (B) PMMA/1% Ca_3Fe; (C) PMMA/5% Ca_3Fe; (D) PMMA/10% Ca_3Fe.

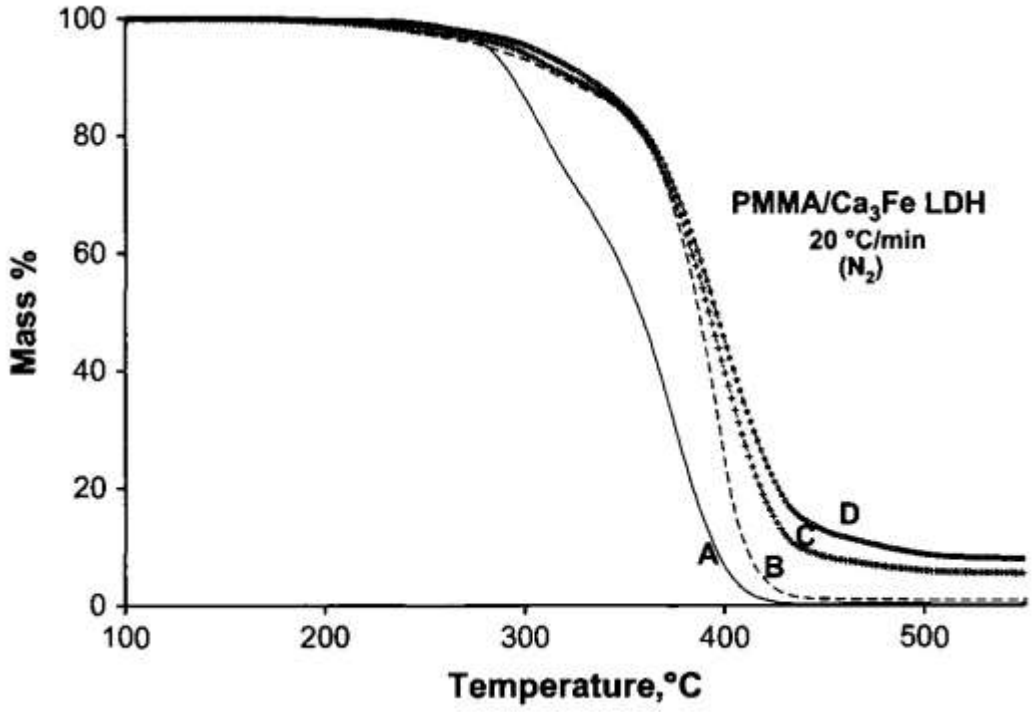

Figure 10: DTG of PMMA and its Ca_3Fe composites.

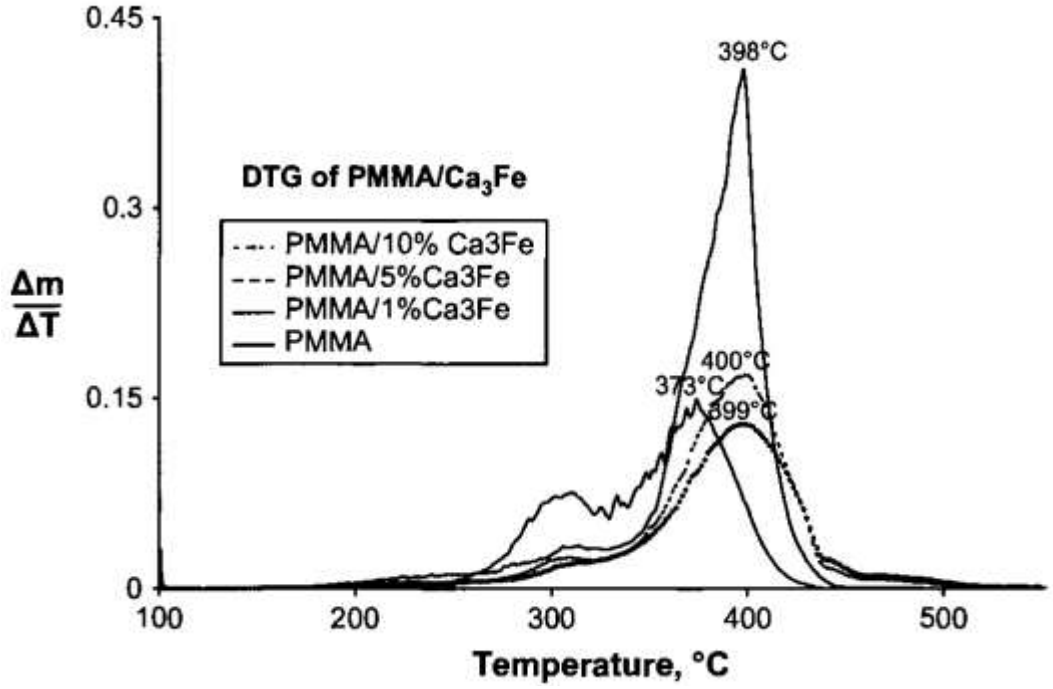

Figure 11:

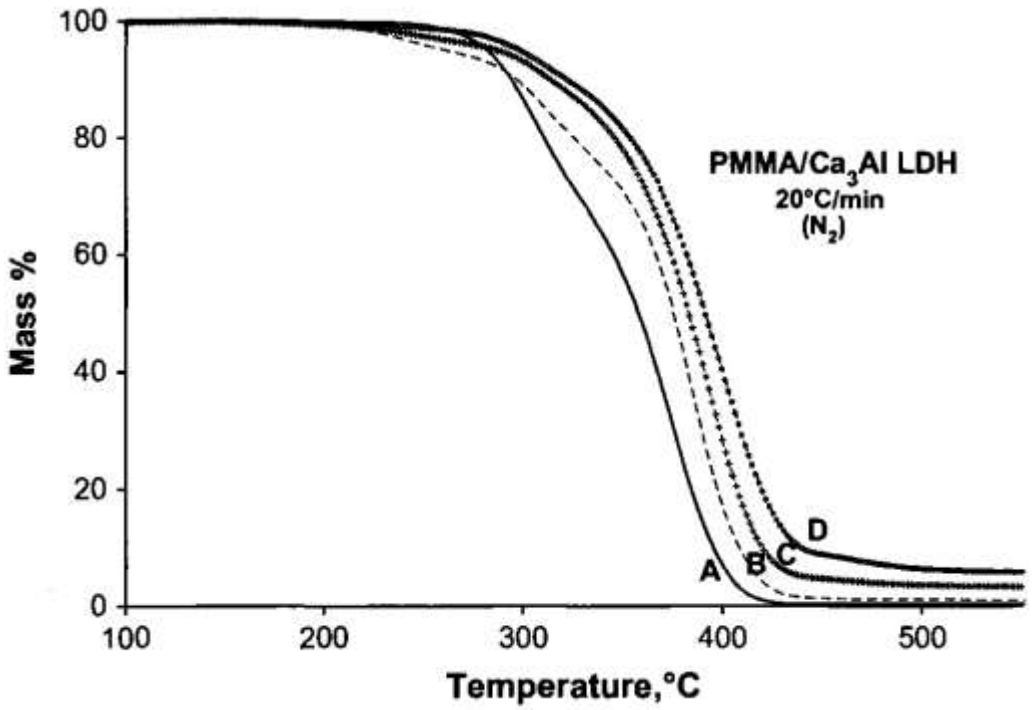

Figure 12: DTG of PMMA/Ca_3Al systems.

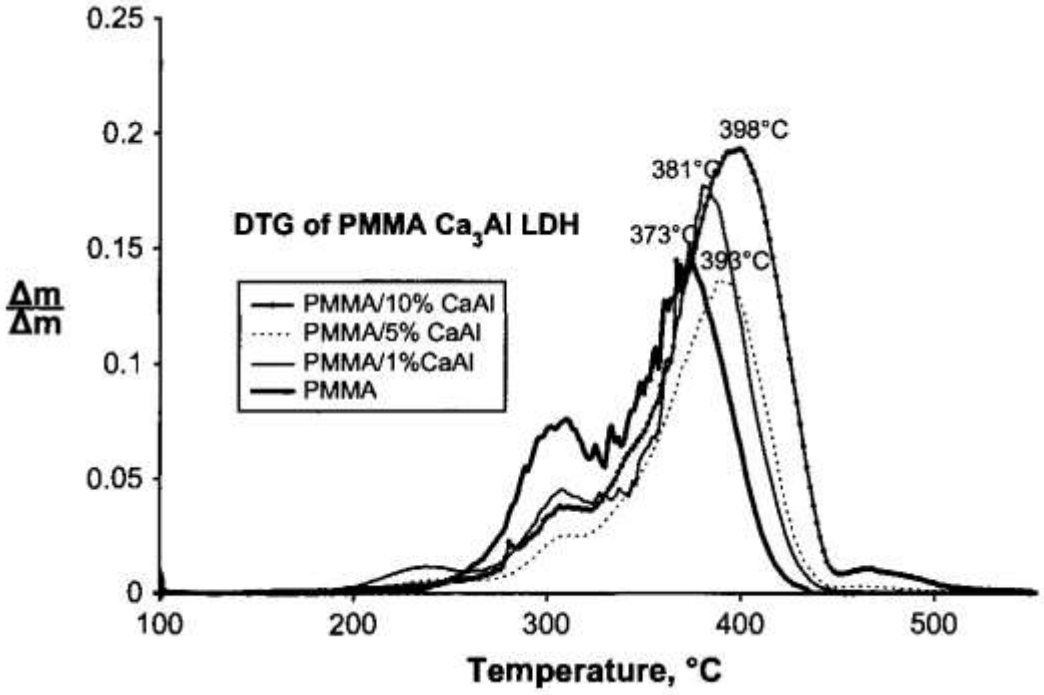

Figure 13: HRR curves of PMMA and PMMA/Ca3Fe composites at 50 kW/m^2. (A) Virgin PMMA; (B) PMMA/5%Ca_3Fe composites; (C) PMMA/10% Ca_3Fe composites.

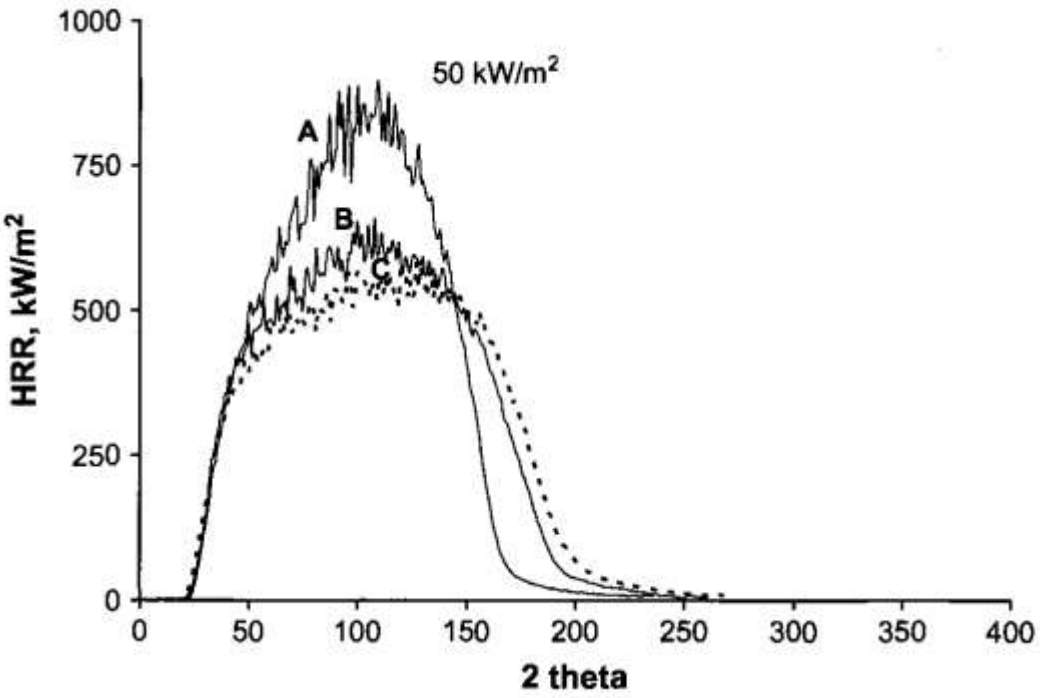

Figure 14: HRR curves of PMMA and PMMA/Ca3Al composites at 50 kW/m^2. (A) Virgin PMMA; (B) PMMA/5%Ca3Al composites; (C) PMMA/10% Ca3Al composites.

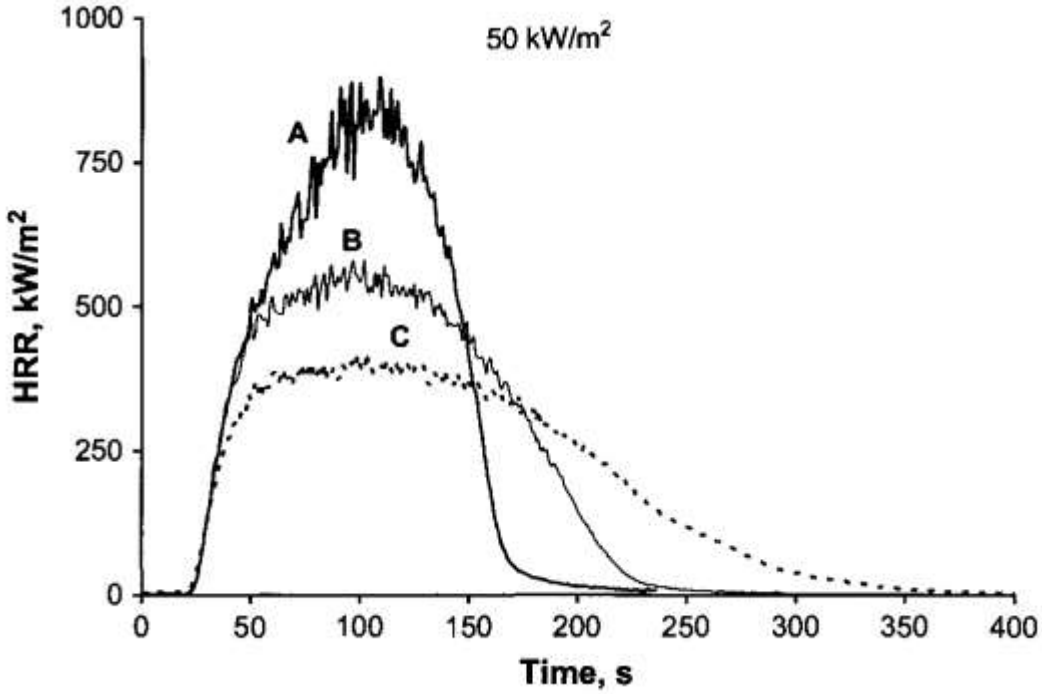

Table 1: TGA summary results of PMMA and its Ca3Al and Ca3Fe composites.

TGA summary data (N_2, 20 °C/min)					
Sample	$T_{0.1}$	ΔT	$T_{0.5}$	ΔT	% Char at 600 °C
PMMA	293	NA	357	NA	0
PMMA/Ca_3Al 1%	296	3	374	17	1
PMMA/Ca_3Al 5%	313	20	382	25	3
PMMA/Ca_3Al 10%	321	28	390	33	5
PMMA/Ca_3Fe 1%	315	22	386	29	1
PMMA/Ca_3Fe 5%	322	29	392	35	4
PMMA/Ca_3Fe 10%	330	37	395	38	6

Note: $T_{0.1}$, temperature of 10% mass loss; $T_{0.5}$, temperature of 50% mass loss, ΔT, difference between virgin polymer and the composite.

Table 2: Cone summary results of PMMA and its Ca3Al and Ca3Fe composites.

Formulation	PHRR (kW/m^2) (% reduction)	THR (MJ/m^2)	ASEA (m^2/kg)	AMLR ($g/s\ m^2$)	t_{ign} (s)
PMMA	902 ± 15 (NA)	79 ± 0	121 ± 3	27.0 ± 0.5	22 ± 3.0
PMMA/Ca_3Fe 1%	780 ± 36 (14)	73 ± 1	137 ± 7	25.4 ± 0.9	20 ± 2.0
PMMA/Ca_3Fe 5%	655 ± 20 (27)	73 ± 0	167 ± 5	21.8 ± 0.5	19 ± 3.0
PMMA/Ca_3Fe 10%	592 ± 13 (34)	72 ± 0	196 ± 13	20.0 ± 0.5	15 ± 0.9
PMMA/Ca_3Al 5%	597 ± 17 (36)	75 ± 2	198 ± 6	19.1 ± 0.9	17 ± 1.1
PMMA/Ca_3Al 10%	418 ± 4 (54)	74 ± 0	215 ± 1	12.9 ± 0.6	17 ± 2.1

Note: PHRR, peak heat release rate; THR, total heat released; ASEA, average specific extension area (smoke); AMRL, average mass loss rate; t_{ign}, time to ignition.

Polymer Degradation and Stability, Vol. 94, No. 4 (April 2009): pg. 705-711. DOI.